




Article

Mechanical Properties of High-Temperature Fiber-Reinforced Thermoset Composites with Plain Weave and Unidirectional Carbon Fiber Fillers

Samuel Ernesto Hall ¹, Victoria Centeno ¹, Sergio Favela ¹, Alexis Lopez ¹, Andrew Gallardo ¹, Jacob Pellicotte ¹, Yulianna Torres ¹, Danielle Coverdell ², Sabrina Torres ², Ahsan Choudhuri ¹, Yirong Lin ^{1,*} and Md Sahid Hassan ^{1,*} 

- ¹ Department of Aerospace and Mechanical Engineering, The University of Texas at El Paso, El Paso, TX 79968, USA; sehallsanchez@miners.utep.edu (S.E.H.); vlcenteno@miners.utep.edu (V.C.); sdfavela@miners.utep.edu (S.F.); alopez125@miners.utep.edu (A.L.); aigallardo@miners.utep.edu (A.G.); jtpellicotte@miners.utep.edu (J.P.); ytorres8@miners.utep.edu (Y.T.); ahsan@utep.edu (A.C.)
- ² Kansas City National Security Campus, Kansas City, MO 64147, USA; dcoverdell@kcncs.doe.gov (D.C.); storres@kcncs.doe.gov (S.T.)
- * Correspondence: ylin3@utep.edu (Y.L.); mhasan2@miners.utep.edu (M.S.H.)



Citation: Hall, S.E.; Centeno, V.; Favela, S.; Lopez, A.; Gallardo, A.; Pellicotte, J.; Torres, Y.; Coverdell, D.; Torres, S.; Choudhuri, A.; et al. Mechanical Properties of High-Temperature Fiber-Reinforced Thermoset Composites with Plain Weave and Unidirectional Carbon Fiber Fillers. *J. Compos. Sci.* **2022**, *6*, 213. <https://doi.org/10.3390/jcs6070213>

Academic Editors: Francesco Tornabene and Thanasis Triantafyllou

Received: 14 June 2022

Accepted: 14 July 2022

Published: 18 July 2022

Publisher's Note: MDPI stays neutral with regard to jurisdictional claims in published maps and institutional affiliations.



Copyright: © 2022 by the authors. Licensee MDPI, Basel, Switzerland. This article is an open access article distributed under the terms and conditions of the Creative Commons Attribution (CC BY) license (<https://creativecommons.org/licenses/by/4.0/>).

Abstract: Fiber-reinforced thermoset composites are a class of materials that address the arising needs from the aerospace and hypersonic industries for high specific strength, temperature-resistant structural materials. Among the high-temperature resistant thermoset categories, phenolic triazine (PT) cyanate esters stand out thanks to their inherent high degradation temperature, glass transition temperature, and mechanical strength. Despite the outstanding properties of these thermosets, the performance of carbon fiber composites using PT cyanate esters as matrices has not been thoroughly characterized. This work evaluated PT and carbon fiber composites' compressive properties and failure mechanisms with different fiber arrangements. A PT resin with both plain weave (PW) and non-crimped unidirectional (UD) carbon fiber mats was analyzed in this research. Highly loaded thermoset composites were obtained using process temperatures not exceeding 260 °C, and the composites proved to retain compressive strength at temperatures beyond 300 °C. Compressive testing revealed that PT composites retained compressive strength values of 50.4% of room temperature for UD composites and 61.4% for PW composites. Post-compressive failure observations of the gage section revealed that the mechanisms for failure evolved with temperature from brittle, delamination-dominant failure to shear-like failure promoted by the plastic failure of the matrix. This study demonstrated that PT composites are a good candidate for structural applications in harsh environments.

Keywords: thermoset composites; phenolic triazine cyanate ester; compressive strength; plain weave; non-crimped unidirectional carbon fiber

1. Introduction

Fiber-reinforced thermoset composites are essential structural materials for advancing hypersonic crafts and structures. Their high stiffness, lightweight, and specific strength afforded through the use of strong matrix and reinforcements make them ideal candidates to support light structures in the hypersonic space. Thermoset composites have been widely implemented in the aerospace [1] and automotive industries [2] thanks to their high thermal and mechanical stability [3,4]. One drawback of the most commonly used thermoset materials is that their polymer networks degrade at temperatures below 340 °C, thus limiting their range of operational temperatures [1]. This has been addressed by developing matrix materials that can withstand high-temperature oxidative environments [5,6]. However, many developed systems lack ease of processability or mechanical properties to be implemented in hypersonic applications.

Cyanate esters are an attractive category of thermoset materials that can address the issues of adopting high-temperature resistant thermosets for industrial composites. As they are cured through self-catalyzed cyclotrimerization, they are easily processable like common thermosets such as epoxies [7]. Moreover, they are high-temperature-resistant thanks to the cyclic triazine rings on their backbone, which results in degradation temperatures close to 450 °C [8]. This category of thermosets has been applied in areas such as RF-transparent shielding [9], electromagnetic interference shielding [10], and high-density energy storage [11]. They have not been widely adopted as structural materials for hypersonic or aerospace. Thus, there is an interest in developing cyanate esters for their implementation as structural materials can withstand the harsh conditions required by the hypersonic field.

One cyanate ester that shows potential as an easily processed and high-performance structural element is the phenolic triazine (PT) type cyanate ester. These materials show ideal glass transition temperatures above 400 °C, given their rigid molecular structures, while simultaneously having low viscosity at low temperatures that allow them to be composited through various resin infusion manufacturing methods [12]. The promising thermal and mechanical properties of PT30 resins have sparked interest from researchers to develop these materials for further implementation in composites. Researchers developed blends of a commercial PT resin with other difunctional cyanate esters to achieve enhanced moisture resistance and long-term thermal stabilities while maintaining the low viscosities that provide easy processability to the resins [13]. Other recent works have shown that PT resins, together with hydroxy and epoxy-functionalized inorganic fillers, could achieve remarkable thermal properties such as a residual char of up to 82% with only 30% inorganic fillers [14]. Thus, the development of PT cyanates is moving towards implementation into composites with high-temperature resistance.

Understanding the mechanical properties of fiber-reinforced composites with PT cyanates is necessary to develop them for structural applications. While the tribological properties of PT cyanate composites have been studied [15], other mechanical properties lack comprehensive study. Their compressive properties are of interest as this is usually the composites' limiting property and design factor [16]. The properties of the matrix and reinforcement, their interfacial interactions, and the influence of geometrical parameters such as the fabric orientation and weaving are all factors that influence the composites' compressive behavior. This work comprised a study of the mechanical properties of cyanate ester composites through the testing of PT 30, a commercial cyanate ester, together with carbon fiber reinforcements in unidirectional and weaved configurations to provide knowledge for the development of high-performance thermoset composites.

2. Methods

2.1. Materials

Primaset (PT 30) cyanate ester resin from Lonza Inc was used as the matrix to manufacture high-performance thermoset composites. Two different reinforcement fabrics were used. The first was plain weave (PW) 3k tow fabrics, and the second was 9 oz/sq. yd non-crimped unidirectional (UD) carbon fabrics. Both reinforcements were obtained from FibreGlast (Brookville, Ohio).

2.2. Vacuum Bag Molding (VBM) Process

Composites of PT30 and two different carbon fabric reinforcements were manufactured through wet layup and a VBM process. First, the individual laminas were laid out by placing sheets of carbon fabric and then spreading the PT30 resin using a roller. To attain an adequate viscosity for spreading and filling the fabrics, the PT30 resin was first heated to 60 °C and then deposited onto the fabrics. Once the layers were laid up, the composites were enclosed in a flexible nylon bagging with a single vacuum connector in a setup shown in Figure 1. The enclosed composites were placed inside a convection oven (Lab Companion OF-01E, Jeio Tech, Seoul, Korea), where heat was applied, and the composites

were placed under a vacuum inside the nylon bag. A maximum vacuum pressure of 78 kPa was applied. After the vacuum pressure was implemented, the PT 30 resin inside the composites was cured following a procedure suggested by the manufacturer. The curing schedule consisted of first preheating the composites to 100 °C for 30 min to allow degassing. Next, the temperature was raised to 150 °C and held for one hour. Following that step, the temperature was raised to 200 °C and held for three hours to complete the curing inside the vacuum bag. Following this process, composites were removed from the nylon bag and post-cured by holding at 260 °C for one hour without applying pressure.

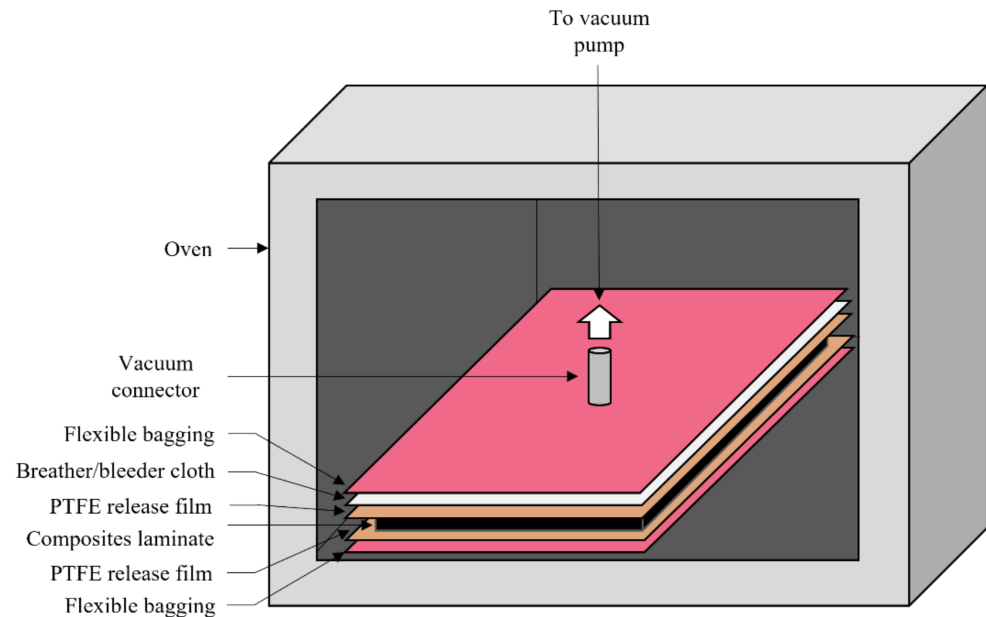


Figure 1. Schematic setup for the VBM process.

Two different types of composites were manufactured for this research. The first were composites with UD fabrics and the second were composites with PW fabrics. The UD composites were fabricated using six layers of fabric aligned in the same direction, i.e., $[0]_6$. The PW composites were manufactured using ten layers of fabric and aligned with the warp fibers in the same direction.

2.3. Composites' Characterization

The quality of the manufactured composites was characterized by measuring their densities, fiber volume fractions, and void volume fractions. The density of the composites was tested according to ASTM D792, which employed the Archimedes method. The fiber and volume fractions of the composites were obtained through measurement of the constituent densities (using ASTM D792) and measuring their initial and final masses after digestion of the matrix using an acid solution. The fiber volume fraction and void volume fractions were calculated based on Equations (1)–(3) below.

$$V_r = (m_f/m_i) \times (\rho_c/\rho_r) \times 100 \tag{1}$$

$$V_m = ((m_i - m_f)/m_i) \times (\rho_c/\rho_m) \times 100 \tag{2}$$

$$V_v = 100 - (V_r + V_m) \tag{3}$$

where V_r , V_m , and V_v represent the reinforcement fiber, matrix, and void volume fractions, respectively; ρ_r , ρ_m , and ρ_c represent the densities of the reinforcement, the matrix, and the composites obtained through the Archimedes method, respectively; and m_i and m_f represent the initial and final masses of the composites, respectively.

To perform the digestion, pieces cut from composites with approximately one gram of mass were placed in beakers containing 25 mL of 95–98% sulfuric acid (Sigma-Aldrich, St. Louis, MO, USA). Next, the solutions were heated using a plate temperature of 240 °C for 1 h 30 min. Following this, 30 mL of 30% hydrogen peroxide (Sigma-Aldrich, St. Louis, MO, USA) was added slowly until the PT30 matrix was fully digested. After the matrix was digested, the fibers were washed with deionized water and dried in an oven before their final mass measurement. The average of three measurements for each composite was reported.

Finally, the composite's thermomechanical properties were measured through dynamic mechanical analysis using a DMA850 from TA Instruments. The testing consisted of flexural loading through a double cantilever clamp. A 10 μm displacement with a 1 Hz frequency was constantly applied, and the temperature was raised at a rate of 3 °C/min up to the degradation temperature of 450 °C. The glass transition temperature was determined to be the temperature at the onset of storage modulus drop.

2.4. Compression Testing and Failure Characterization of PT 30 Composites

The compressive properties of carbon-fiber-reinforced PT 30 composites were obtained through testing according to ASTM D6641. This method used a combined loading compression (CLC) fixture from Wyoming Fixtures. A total of 10 specimens were cut from each composite. Each specimen had a width of 12.7 mm and a length of 139.7 mm. The samples were cut with their length parallel to the main fiber direction for the case of UD composites, and parallel to the main warp fibers in PW composites. Woven composites were tested without tabs, but UD composites were bonded to square-ended tabs to ensure acceptable failure modes. The tabs had the same width as the specimens and had lengths of 63.5 mm, resulting in 12.7 mm long gage sections in the middle of the specimens. Woven fiberglass sheets were used as the tabbing materials for testing at temperatures of 200 °C and below. For tests performed at 300 °C, stainless steel tabs were used. The bonding materials consisted of Loctite EA 9394C-2QT AERO from Loctite for tests up to 200 °C and Duralco 4700 from Cotronics Corp for testing at 300 °C.

Room temperature tests and elevated temperature tests at 100 °C, 200 °C, and 300 °C were performed for both PW and UD composites. All tests were performed using an Instron 68TM-50 universal testing frame with a 50 kN capacity. The elevated temperature tests were performed inside an Instron 3119-600 series environmental chamber. The fixture was placed inside the chamber, and the temperature was held for 30 min at the setpoint before testing to ensure temperature uniformity.

The compressive strength of the composites and their compressive modulus were obtained from the average of five testing specimens for each temperature and fiber configuration. The compressive modulus was obtained according to ASTM D6641 from the chord modulus between 0.01% and 0.03% strain. The characteristics of the compressive failure of the different composites were studied by observing the failed gage section using a scanning electron microscope (SEM) (Phenom Pro X, Thermo Fisher Scientific, Waltham, MA, USA). Before microscopy, the specimen's gage sections were cut and polished lightly; thus, the edges of the composites were not captured.

3. Results and Discussions

3.1. Manufactured Composites' Quality

Fiber-reinforced composites of a high-performance PT cyanate ester matrix and two different types of carbon fiber arrangements were successfully manufactured through VBM. The resultant densities, fiber fractions, and void fractions are shown in Table 1. The densities of the UD composites were lower than those of PW composites. This was because of greater compaction in PW composites compared with UD composites during the VBM process, as it has been found that woven fabrics have higher through-thickness and in-plane resin permeabilities compared with non-crimp fabrics in the range of the presently applied consolidation pressures [17]. Despite having lower fiber fractions than the PW composites,

the UD composites had fiber fractions in a range where mechanical compressive failure was expected to result from the combined effects of fiber and matrix and not be dominated by the properties of the matrix.

Table 1. Properties of VB-molded PT30/carbon fiber composites.

Composites	Density (g/cm ³)	Fiber Fraction (%)	Void Fraction (%)
UD1	1.37	49.59	6.23
UD2	1.32	39.71	6.60
UD3	1.28	24.34	3.34
PW1	1.46	59.86	2.80
PW2	1.41	57.41	5.85
PW3	1.50	61.08	0.06

The low available consolidation pressures (<78 kPa) of the VBM process resulted in defects such as voids found in both UD and PW composites. High void contents of up to 6.60% were present in the manufactured composites and were more significant in UD than in PW composites. Moreover, UD composites attained lower fiber fractions with an average of $37.88 \pm 10.39\%$. The higher resistance to resin flow during consolidation for UD fabrics than PW fabrics produced pockets of air inside the laminates that could not be filled with the vacuum pressure. The resulting voids in the composites were expected to reduce the mechanical properties of the composites through the initiation of premature cracks and reduction of structural material in the loading cross-section [18].

3.2. Compressive Properties of PT30 Composites at Room Temperature

The compressive properties of PT 30 composites with PW and UD fibers were tested and compared. Figure 2 shows the average compressive strengths of three UD and three PW composites obtained at room temperature for the different composites manufactured. There was a more extensive spread in the strengths of the different UD composites compared with the PW composites due to the larger variations of volumetric fiber fractions exhibited. There was no clear relationship between the void volume fractions and the compressive strength of the UD composites, as there were UD composites with high strength despite having the highest void content. However, the PW composite with the highest strength was the one with the lowest fraction of voids, clearly showing that the reduction of voids was a factor in the increase in strength for PT30 composites. The attained compressive strengths of UD composites, which were highest at 542 ± 76 MPa, were lower compared with similar composites manufactured through methods such as an autoclave molding (674 MPa) [19], but were higher than other composites manufactured through techniques such as vacuum infusion (420 MPa) [20].

The UD and PW composites with the highest compressive strengths were analyzed through TGA tests (Figure 3). Both composites showed promising thermal stability with only 1 wt% mass loss at 146.63 °C for UD2 samples. On the other hand, for PW3 samples, the degradation onset point (1% weight loss) was obtained at 288.46 °C. High thermal stability of PW3 was achieved as a result of having the lowest amount of fraction of voids in the PW3 composite.

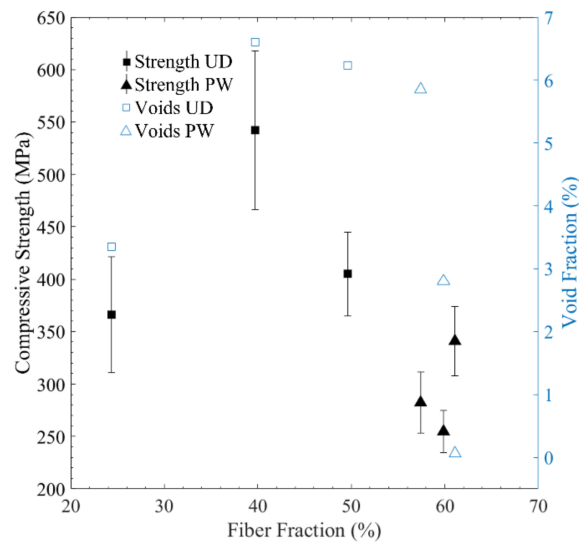


Figure 2. Compressive strengths of manufactured PT 30 composites with UD and PW fibers at room temperature.

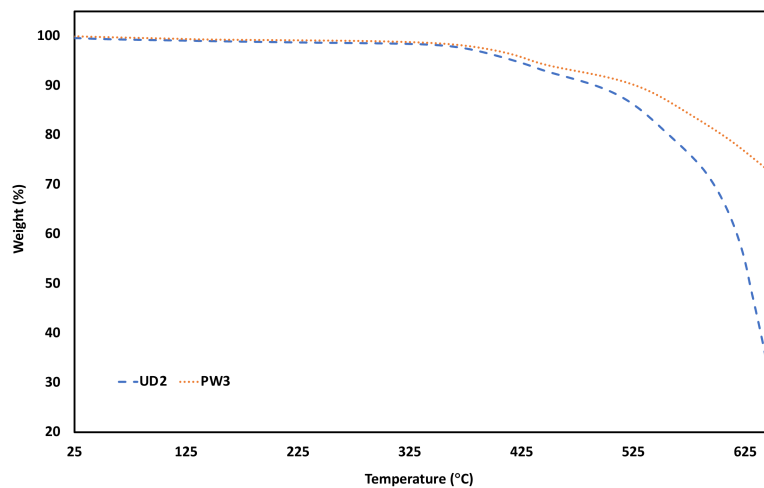


Figure 3. Thermogravimetric analysis (TGA) of manufactured PT 30 composites with UD and PW fibers in an air environment.

The compressive strengths of PT30 composites at elevated temperatures were studied to confirm their potential as high-performance structural elements. As observed in Figure 4, the manufactured PW and UD composites were affected in different magnitudes by the increased environmental temperature during compression testing. At 100 °C, UD composites exhibited strengths of 89.26% of the room temperature value, whereas the PW composites retained 79.87% of their strength. At such low temperatures, matrix softening was not expected to contribute to the reduction in the composites’ strengths. This would support the higher degree of weakening for PW composites over UD composites as the fiber arrangements contain a higher interfacial area. As the temperature increased to 200 °C and 300 °C, the PW composites showed increased retention of compressive strength when compared with UD composites. The reduced compressive strengths of UD composites were most likely the result of the softening of the PT30 matrix as a result of it approaching its T_g , which was measured through DMA to be 378 °C. Compressive failure models that consider that failure initiates as a result of micro-buckling of misaligned fibers in the plastic matrix have proven to be accurate at estimating composites’ compression strengths [21]. Micro-buckling was more likely to initiate as the matrix softened as a result of increased temperatures. PW composites had an increased residual strength compared with UD

composites because the fill fiber bundles of the weave provided lateral support that delayed micro-buckling initiation. UD composites, however, only had neighboring axial fiber bundles to support them laterally, which were far away from each other and thus had a reduced strengthening effect.

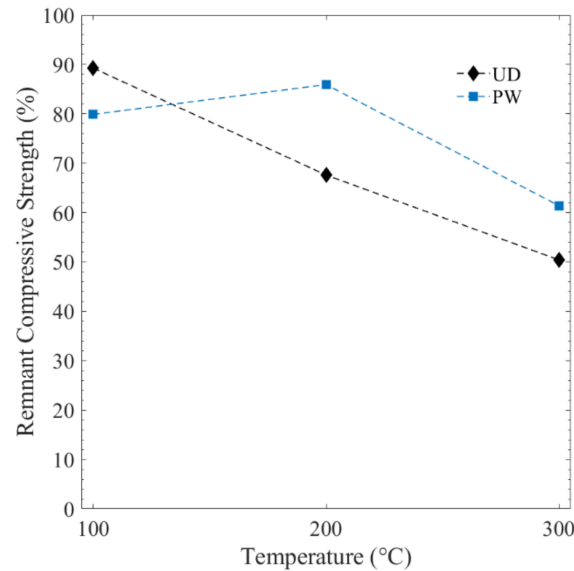


Figure 4. Remnant compressive strength (expressed as a percentage of strength at room temperature) of PW and UD PT 30 composites.

The modulus of the PT30 composites with PW and UD fibers evolved with temperature differently to their compressive strength. Figure 5 shows that UD composites retained 97.5% of the room temperature compressive modulus at 100 °C and retained about 60.61% of their modulus at 300 °C. In contrast, PW composites showed a reduced compressive modulus of only 56.74% at 100 °C, which dropped at a lower rate than UD composites, down to 41.38% of its room temperature value at 300 °C. The difference in the reduction of compressive modulus between PW and UD composites could be best explained as being proportional to the effective matrix contributions for each fiber arrangement. In UD composites, all fibers were aligned to the applied compressive load.

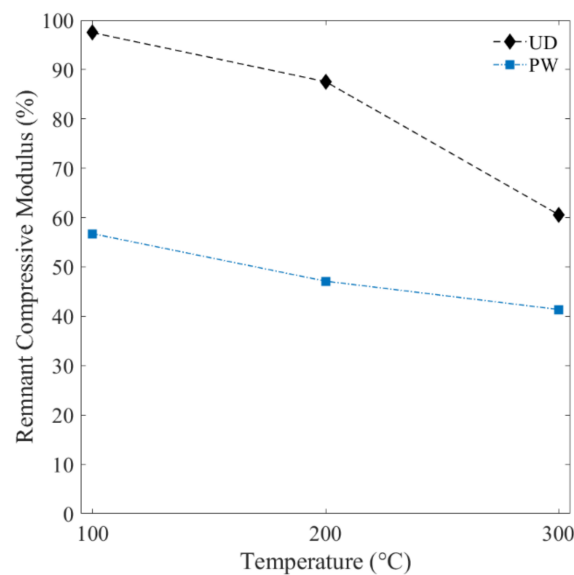


Figure 5. Remnant compressive modulus (expressed as a percentage of modulus at room temperature) of PW and UD PT 30 composites.

In contrast, in PW composites, only half of the fibers corresponding to the axially oriented fibers directly contributed to the load response. The transverse fiber bundles in the PW composites had an elastic response determined mainly by the PT30 matrix, which softened as the temperature increased. The significant drop in the magnitude of the modulus for PW composites at 100 °C was believed to not only be a result of the softening of the matrix, but also of other contributions such as the evolution of the fiber and matrix interfaces with temperature. Softening of the interface, which could be a region with a higher modulus than the bulk, with temperature could explain the drastic reduction in compressive modulus for the PT 30 composites [22].

3.3. Effect of Environmental Testing Temperature on Compression Failure Modes in UD and PW Composites

The failure sections of compression testing specimens were observed through SEM to understand the mechanisms of failure and their evolution with temperature for the different carbon fiber arrangements. Figure 6 shows the failed gage sections of PW composites from room temperature up to 300 °C. From Figure 6a, it could be seen that, at room temperature, the PW composites seemed to fail through the formation of a wedge with an inclination of 21.3° from the axial direction. The wedge formed as a result of delamination in the composite and brittle cracking of the matrix, followed by fiber bundle breakage from the edges towards the center. There have been reports of wedge-like failures in composites with brittle matrices with manufacturing imperfections such as cracks [23]. The manufacturing imperfections and the brittleness of the PT30 matrix were likely the cause of failure for PW composites at all of the tested temperatures.

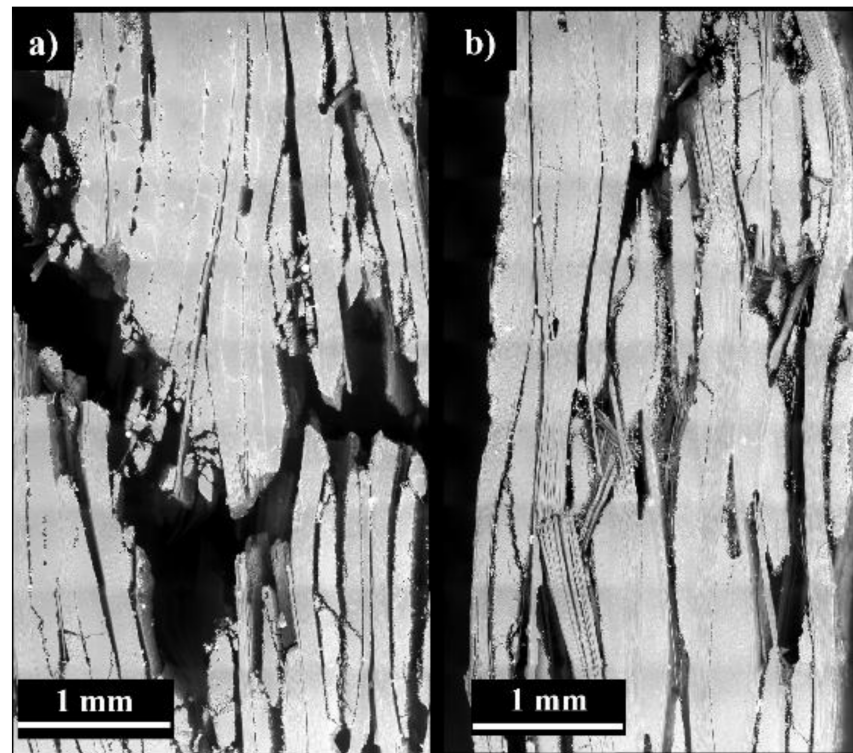


Figure 6. Cont.

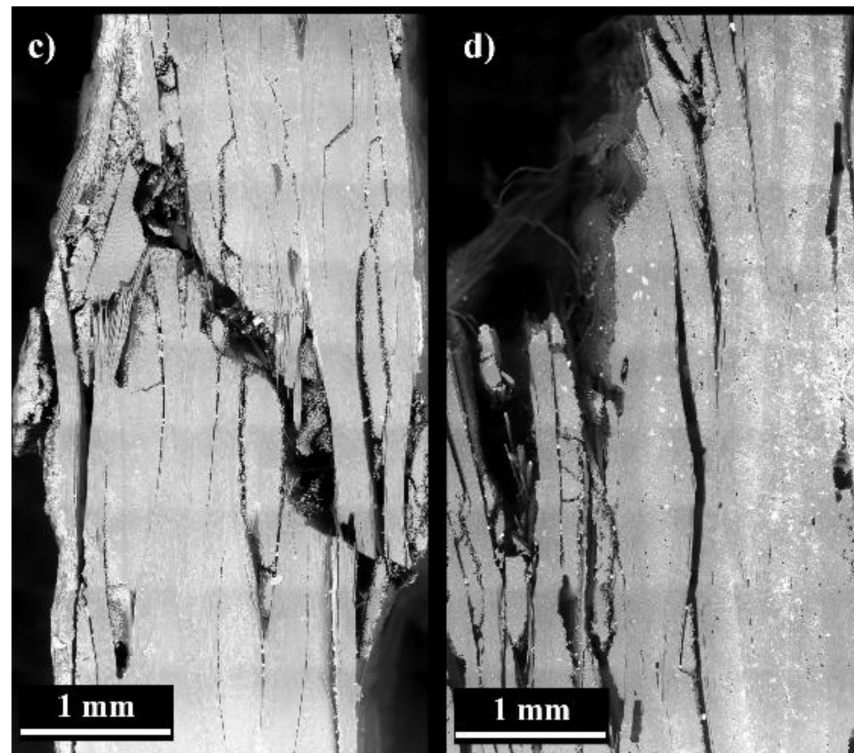


Figure 6. SEM images of the gage section of PW composites after compression testing under different environmental temperatures: (a) room temperature, (b) 100 °C, (c) 200 °C, and (d) 300 °C.

The testing temperature influenced the PW composites' failure modes. From the Figure 6b, it could be observed that, at 100 °C, there was a high prevalence of delamination. The delamination caused intralaminar cracks along with the transverse fiber bundles, similar to what has been observed by other researchers on delamination buckling failure [24]. Figure 6b–d showed that, as the testing temperature increased, composites appeared to fail along a defined off-axis direction, like a shear failure of isotropic materials. The off-axis angle of shear failure increased from 14.08° at 100 °C to 29.45° at 200 °C, and then dropped to 26.47° at 300 °C. This was likely due to the softening of the PT 30 matrix and the yielding as a result of shear forces exerted by the wavy fiber bundles in the PW arrangement. With the presence of delamination above and below (with respect to the axial direction), the main failures were evident throughout all specimens. The prevalence of delaminations indicated that manufacturing defects arising from the high void contents (up to 5.85%) contributed to the compressive failure.

SEMs of UD composites' compression specimens tested under different environmental temperatures are shown in Figure 7 below. A clear difference was identified in the failed sections' shape between the room and elevated temperatures. As seen in Figure 7a, at room temperature, no through-thickness failure band was observed. Instead, translaminar cracks were seen at various heights along the axial direction. Delaminations were also prevalent throughout the thickness of the UD composites at room temperature. The prevalent delaminations were likely the main contributor to failure. It was hypothesized that, at room temperature, the compressive stress necessary to expand the interlaminar cracks, which were a result of voids from the VBM process, was lower than the stress required to yield the matrix and initiate micro buckling. Therefore, as the temperature of the compression testing environment increased and the matrix approached its glass transition temperature, matrix yielding could occur before the growth of interlaminar cracks and result in shear-like failure through the thickness of the composites. As seen in Figure 7b, the UD composites at 100 °C continued to show delamination through their thickness, but to a lesser degree than the composites at room temperature. The reduction in delaminations allowed for a

wedge-like failure to originate through the thickness of the UD composites. Figure 7c,d show that, at elevated temperatures of 200 °C and 300 °C, there was a shift in the failure mode towards a through-thickness shear-like failure. This was expected because of the PT30 matrix softening with temperature. As the UD composites did not contain fill fiber bundles in the transverse direction, there was less resistance to the propagation of the shear crack through the thickness of the composites. Thus, the shear crack appeared to follow a single direction without many interruptions in the UD composites. The composites at 200 °C and 300 °C had off-axis angles of shear failure of 29.74° and 14.17°, respectively.

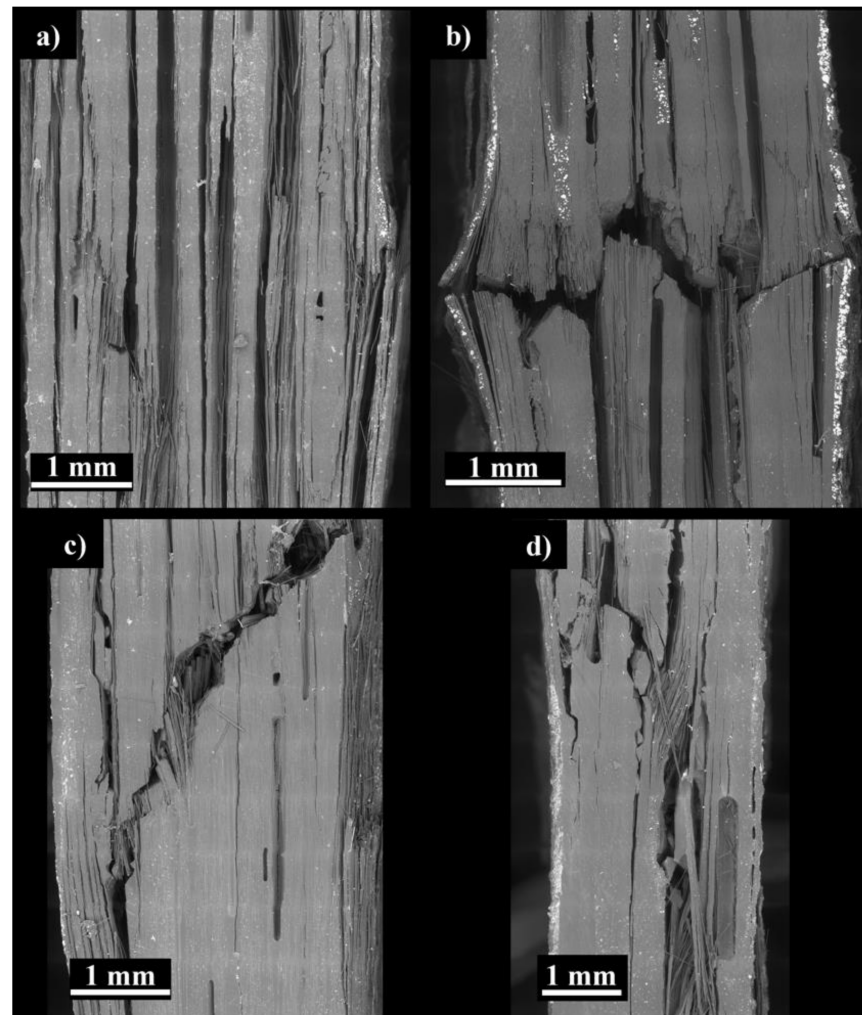


Figure 7. SEM images of the gage section of UD composites after compression testing under different environmental temperatures: (a) room temperature, (b) 100 °C, (c) 200 °C, and (d) 300 °C.

4. Conclusions

The mechanical properties of fiber-reinforced composites with a high-performance cyanate ester resin were studied under elevated temperatures. The strengths of the composites dropped as temperature increased regardless of the fiber arrangement selected. The lack of fiber surface functionalization for compatibility with the carbon fiber reinforcements likely resulted in weakened interphases that contributed to the reduction in compressive strength at temperatures below the glass transition temperature. It was also identified that the fiber arrangement in PT composites impacted the reduction in strength as the operating temperature increased. Woven fibers had a higher remnant strength at higher temperatures than unidirectional fibers because of the anti-buckling supporting effect of the transverse fill fibers. Despite their reduced strengths, the manufactured PT30 and carbon fiber composites

from this work retained more than 50% of their room temperature strength at temperatures of 300 °C. TGA tests also proved the thermal stability of woven fiber composites. A closer analysis of the failure section revealed that the failure mechanisms shifted from delamination to shear-like failure at temperatures more than 100 °C below the T_g of the composites' matrix. The analysis revealed that, in VBM composites, failure is initiated by the growth of cracks from the initial void defects when the matrix and filler are high-strength materials. Because of this, VBM composites' strength modeling must incorporate the effect of voids obtained in the manufacturing process. This study demonstrated that PT composites are suitable structural materials for high-temperature environment applications.

Author Contributions: Conceptualization, S.E.H., Y.L. and M.S.H.; methodology, S.E.H., A.L., V.C., J.P., Y.T. and S.F.; software, S.E.H.; validation, S.E.H., A.G., Y.L. and D.C.; formal analysis, S.E.H.; investigation, Y.L.; resources, A.C. and Y.L.; data curation, S.E.H.; writing—original draft preparation, S.E.H.; writing—review and editing, M.S.H.; visualization, S.T. and Y.L.; supervision, Y.L.; project administration, S.T. and Y.L.; funding acquisition, Y.L. All authors have read and agreed to the published version of the manuscript.

Funding: This work was supported by the US Department of Energy's National Nuclear Administration under Grant No. DE-NA-0004015.

Conflicts of Interest: The authors declare no conflict of interest.

References

1. Hamerton, I.; Mooring, L. 7-The use of thermosets in aerospace applications. In *Thermosets*; Guo, Q., Ed.; Woodhead Publishing: Sawston, UK, 2012; pp. 189–227. ISBN 978-0-85709-086-7. [\[CrossRef\]](#)
2. Mallick, P.K. Chapter 6-Thermoset matrix composites for lightweight automotive structures. In *Materials, Design and Manufacturing for Lightweight Vehicles*, 2nd ed.; Mallick, P.K., Ed.; Woodhead Publishing: Sawston, UK, 2021; pp. 229–263. ISBN 978-0-12-818712-8.
3. Hassan, M.S.; Billah, K.M.M.; Hall, S.E.; Sepulveda, S.; Regis, J.E.; Marquez, C.; Cordova, S.; Whitaker, J.; Robison, T.; Keating, J.; et al. Selective Laser Sintering of High-Temperature Thermoset Polymer. *J. Compos. Sci.* **2022**, *6*, 41. [\[CrossRef\]](#)
4. Chavez, L.A.; Ibañez, P.; Hassan, S.; Hall-Sanchez, S.E.; Billah, K.M.M.; Leyva, A.; Marquez, C.; Espalín, D.; Torres, S.; Robison, T.; et al. Low-temperature selective laser sintering 3D printing of PEEK-Nylon blends: Impact of thermal post-processing on mechanical properties and thermal stability. *J. Appl. Polym. Sci.* **2022**, *139*, 52290. [\[CrossRef\]](#)
5. Bulgakov, B.; Sulimov, A.; Babkin, A.; Timoshkin, I.; Solopchenko, A.; Kepman, A.; Avdeev, V. Phthalonitrile-carbon fiber composites produced by vacuum infusion process. *J. Compos. Mater.* **2017**, *51*, 4157–4164. [\[CrossRef\]](#)
6. Sun, B.-G.; Lei, Q.; Guo, Y.; Shi, H.-Q.; Sun, J.-B.; Yang, K.-X.; Zhou, H.; Li, Y.-Q.; Hu, N.; Wang, H.; et al. Enhanced mechanical properties at 400 °C of carbon fabric reinforced phthalonitrile composites by high temperature postcure. *Compos. Part B Eng.* **2019**, *166*, 681–687. [\[CrossRef\]](#)
7. Hamerton, I. *Chemistry and Technology of Cyanate Ester Resins*; Springer Science & Business Media: Berlin/Heidelberg, Germany, 2012; ISBN 978-94-011-1326-7.
8. Ramirez, M.L.; Walters, R.; Lyon, R.E.; Savitski, E.P. Thermal decomposition of cyanate ester resins. *Polym. Degrad. Stab.* **2002**, *78*, 73–82. [\[CrossRef\]](#)
9. Liu, Z.; Zhang, J.; Tang, L.; Zhou, Y.; Lin, Y.; Wang, R.; Kong, J.; Tang, Y.; Gu, J. Improved wave-transparent performances and enhanced mechanical properties for fluoride-containing PBO precursor modified cyanate ester resins and their PBO fibers/cyanate ester composites. *Compos. Part B Eng.* **2019**, *178*, 107466. [\[CrossRef\]](#)
10. Ren, F.; Song, D.; Li, Z.; Jia, L.; Zhao, Y.; Yan, D.; Ren, P. Synergistic effect of graphene nanosheets and carbonyl iron–nickel alloy hybrid filler on electromagnetic interference shielding and thermal conductivity of cyanate ester composites. *J. Mater. Chem. C* **2018**, *6*, 1476–1486. [\[CrossRef\]](#)
11. Zhang, X.; Yuan, L.; Guan, Q.; Liang, G.; Gu, A. Greatly improving energy storage density and reducing dielectric loss of carbon nanotube/cyanate ester composites through building a unique tri-layered structure with mica paper. *J. Mater. Chem. A* **2017**, *5*, 21909–21918. [\[CrossRef\]](#)
12. Janković, B. Thermal degradation process of the cured phenolic triazine thermoset resin (Primaset® PT-30). Part I. Systematic non-isothermal kinetic analysis. *Thermochim. Acta* **2011**, *519*, 114–124. [\[CrossRef\]](#)
13. Tsiamis, A.; Iredale, R.J.; Backhouse, R.; Hallett, S.R.; Hamerton, I. Liquid Processable, Thermally Stable, Hydrophobic Phenolic Triazine Resins for Advanced Composite Applications. *ACS Appl. Polym. Mater.* **2019**, *1*, 1458–1465. [\[CrossRef\]](#)
14. Goyal, S.; Forrester, M.J.; Coverdell, D.; Torres, S.; Lee, M.W.; Cochran, E.W. High-Temperature-Performance Cyanate Ester Composites with Carboranes. *Macromolecules* **2021**, *54*, 9155–9164. [\[CrossRef\]](#)
15. Bajpai, A.; Saxena, P.; Kunze, K. Tribo-Mechanical Characterization of Carbon Fiber-Reinforced Cyanate Ester Resins Modified with Fillers. *Polymers* **2020**, *12*, 1725. [\[CrossRef\]](#) [\[PubMed\]](#)

16. Mechin, P.-Y.; Keryvin, V.; Grandidier, J.-C. Effect of the nano-filler content on the compressive strength of continuous carbon fibre/epoxy matrix composites. *Compos. Part B Eng.* **2021**, *224*, 109223. [[CrossRef](#)]
17. Comas-Cardona, S.; Binetruy, C.; Krawczak, P. Unidirectional compression of fibre reinforcements. Part 2: A continuous permeability tensor measurement. *Compos. Sci. Technol.* **2007**, *67*, 638–645. [[CrossRef](#)]
18. Bowles, K.J.; Frimpong, S. Void Effects on the Interlaminar Shear Strength of Unidirectional Graphite-Fiber-Reinforced Composites. *J. Compos. Mater.* **1992**, *26*, 1487–1509. [[CrossRef](#)]
19. Kirmse, S.; Kim, K.; Ranabhat, B.; Hsiao, K.-T. Effects of carbon nanofiber z-threads on the longitudinal compressive strength of unidirectional cfrp laminates. In Proceedings of the SAMPE 2019, Charlotte, NC, USA, 20–23 May 2019; Available online: <https://par.nsf.gov/biblio/10096112> (accessed on 11 June 2022).
20. Uddin, M.F.; Sun, C.T. Strength of unidirectional glass/epoxy composite with silica nanoparticle-enhanced matrix. *Compos. Sci. Technol.* **2008**, *68*, 1637–1643. [[CrossRef](#)]
21. Moran, P.M.; Liu, X.H.; Shih, C.F. Kink band formation and band broadening in fiber composites under compressive loading. *Acta Metall. Mater.* **1995**, *43*, 2943–2958. [[CrossRef](#)]
22. Reed, K.E. Dynamic mechanical analysis of fiber reinforced composites. *Polym. Compos.* **1980**, *1*, 44–49. [[CrossRef](#)]
23. Wang, Y.; Zhang, J.; Zhang, J.; Zhou, Z.; Fang, G.; Wang, S. Compressive behavior of notched and unnotched carbon woven-ply PPS thermoplastic laminates at different temperatures. *Compos. Part B Eng.* **2018**, *133*, 68–77. [[CrossRef](#)]
24. Opelt, C.V.; Cândido, G.M.; Rezende, M.C. Fractographic study of damage mechanisms in fiber reinforced polymer composites submitted to uniaxial compression. *Eng. Fail. Anal.* **2018**, *92*, 520–527. [[CrossRef](#)]